NATIONAL ADVISORY COMMITTEE FOR AERONAUTICS

TECHNICAL MEMORANDUM

No. 1096

INVESTIGATION OF TURBULENT MIXING PROCESSES

By K. Viktorin

Forschung auf dem Gebiete des Ingenieurwesens
Vol. 12, No. 1, January - February, 1941

Washington
October 1946

NATIONAL ADVISORY COMMITTEE FOR AERONAUTICS

TECHNICAL MEMORANDUM NO. 1096

INVESTIGATION OF TURBULENT MIXING PROCESSES[1]

By K. Viktorin

SUMMARY

With water as driving medium and delivered medium in a device similar to a simple jet apparatus, the pressure and velocity fields of the mixing zone were explored with a pitot bar; the ratio of delivered to driving volume ranged between the values 0, 1, 2, and 4.

An attempt was also made to analyze the mixing flow mathematically by integration of the equation of motion, with the aid of conventional formulas for the turbulent shearing stress, but this succeeded only approximately for the very simplified case that a driving jet is introduced in an unlimited parallel flow, while the pressure over the whole mixing field is assumed to be constant (pt. 2).

In spite of these dissimilar assumptions for the theory and the experiment, the form of the measured and the computed velocity profiles indicates a very high degree of approximation (fig. 22).

The pressure rise, which was approximated by Flügel's formulas, disclosed good agreement with the measured values (fig. 25).

INTRODUCTION

Surveys of turbulent mixing fields published so far deal only with fields of practically constant pressure (although Forthmann (reference 1) presents an experimental arrangement where pressure and velocity are measured in a completely closed, abruptly diverging channel, but fails to give any details about the results of the pressure measurement).

The principal object of the present investigation therefore is to

---

[1] "Untersuchung turbulenter Mischvorgänge." Forschung auf dem Gebiete des Ingenieurwesens, vol. 12, no. 1, Jan./Feb. 1941, pp. 16-30.

survey mixing fields with variable pressure, similar to those prevailing for a jet apparatus.

A further aim was the prediction of such mixing fields on the basis of Prandtl's formula for turbulent shearing stress, but this was successful only under considerable limitations on account of the mathematical difficulties involved.

Lastly, a simplified method of calculation for turbulent mixing processes was checked for agreement with reality against the measurements.

EXPERIMENTAL METHOD

Experimental Setup

The size of the arrangement was chosen with a view of making the survey apparatus which was used for measuring the pressure and velocity of the water serving as test fluid, small enough so that its presence caused no appreciable disturbance in the attitude of the flow, while a certain minimum size of the survey apparatus is necessary for reasons of manufacture and experimental manipulation.

The order of magnitude of the utilized velocities is dictated by the demand for convenient experimental manipulation and absence of special difficulties in the positive and negative pressures anticipated during the measurement. Furthermore, the velocity head corresponding to the maximum velocity was to be realizable within the available building space, because it was expedient for the attainment of a uniform state of flow to produce this velocity by means of overhead tank with free surface.

The setup is illustrated in figures 1 and 2. A pump driven by electric motor pumps the water out of the filled reservoir 1, through the suction and pressure line 2 and 3 into an overhead tank 4. An overflow 5 ensures - independent of the speed fluctuations of the pump - a constant pressure head for the jet and for the supply of the delivered water volume (secondary water), which is measured by a test nozzle 8 at the end of the supply line. The jet leaves the driving nozzle 9 at a speed of around 10 meters per second, mixes with the surrounding water in the cylindrical mixing chamber 13 while giving off momentum and carries it along with it. The mixture gains the outside at the end of the mixing chamber through holes 15 in the envelope of the mixing pipe 14, flows downward through a branch 16, passes through throttle valve 17, and back into reservoir 1. The water level in the reservoir is so high that valve 17 is under water; this prevents disagreeable splashing of the outflowing water jet. For the same purpose the level in the supply

tank 22 for the secondary water is also maintained high enough by appropriate throttle-valve setting to keep the mouth of the nozzle under water. The kinetic energy of the outgoing secondary water stream is dissipated in a small swash chamber 19. Straightener and screens 20 then provide for a uniform inflow to the driving jet. Arranged directly around the jet, a narrow-cell straightener 21 (fig. 2) with radial ribs ensures the elimination of circumferential components. To avoid rotation in the driving jet the supply line 6 to the driving nozzle is likewise fitted with a straightener 10. Different secondary water volumes are obtained with different test nozzles 8. The quantity of driving water is the same for all tests.

The measuring instrument is a long pitot tube 23 (fig. 2), carrying the actual survey apparatus at the tapered forward end. Aside from the dynamic pressure orifice, it is fitted with lateral orifices for recording the static pressure. Figure 3 illustrates the pitot tube and its particular tip. Rubber tubing serves as lead to the water and mercury manometers. Throttles and glass vessels acting as air chambers are mounted in the test lines to dampen the occasionally violent pressure fluctuations. The pitot tube is suspended by rings 24 and small metal strips 25 (fig. 2) from a strong iron beam 26 which, together with the suspended impact tube, can be moved vertically up or down by means of a nut and spindle 27. The height position for each spindle is read on a scale 28. The rings and strips which, on backward shifting of the pitot tube, came directly before or behind the test orifices, are removed. Distance pieces and welded-on stops 29 serve for adjusting scale and pointer, as well as control. The rear end of the mixing pipe is closed by a plate 32 through which the pitot tube is introduced by means of a stuffing box, which can be raised or lowered with the pitot tube by hand-wheel and lead screw 33.

Thus, by raising and lowering the pitot tube and by shifting it along its axis, the test orifices can be placed at any desired point of the vertical median plane of mixing chamber, with exception of the area adjacent to the wall, which, however, is of less interest in the study of the mixing processes. A number of test orifices in the horizontal median plane along mixing pipe 14 enables pressure measurements directly at the wall (fig. 4). The position of the pitot tube with respect to a displacement along its axis can also be read by means of scale and pointer 34. The pointer is solidly connected to plate 32; the scale is scratched on the pitot tube.

Calibrations

(a) Overhead tank.- To calibrate the nozzle it was first necessary to gage the overhead tank. To this end it was filled and then emptied in stages, the drained water being weighed and the respective

abatements of the level measured. The mathematically obtained cross-sectional area F_o of the tank showed itself fairly constant over the height in question, hence could be used as constant in the volume determination.

(b) Nozzles.- All nozzles are calibrated by discharge test at the place of utilization. The necessary formulas are briefly outlined (fig. 5). (Subscript 1 refers to start of outflow test, subscript 2 to end of outflow test; differences in height level between start and end of test are indicated with Δ.)

The volume of the outflow at speed C in time interval dt is equal to the decrease in volume in the overhead tank:

$$\alpha F c dt = -F_o dH \tag{1}$$

where α is the outflow coefficient. From the energy equation, applied to cross sections II and III, the outflow velocity C follows at

$$c = \sqrt{\frac{2gh}{1 + \zeta - \epsilon^2}} \tag{2}$$

where ϵ is the cross-section ratio F/F_m and ζ the loss coefficient of the nozzle.

On the premise of constant pipe friction coefficient the energy equation, applied to the sections I and II, gives

$$\frac{dh}{dH} = \frac{h}{H} \tag{3}$$

Integration of equation (1) by means of equations (2) and (3) gives

$$\frac{1}{\alpha F}\sqrt{1 + \zeta - \epsilon^2} = \frac{t\sqrt{2gh_1}}{2F_o H_a\left(1 - \sqrt{\frac{H_2}{H_1}}\right)} = \psi$$

Quantities t, h_1, H_1, and H_2 are determined by test. Herewith the throughflow quantity becomes

$$G = \alpha c F \gamma = \frac{\sqrt{2gh}}{\psi} \gamma$$

Table 1 gives the data for the throughflow quantities in the principal tests for the driving nozzle and the three nozzles employed for the secondary water nozzles; h is the effective pressure head measured in the main test, μ the ratio of secondary water quantity to driving water quantity, which approximates the values 0, 1, 2, and 4 for the four principal test series.

TABLE 1.- RECORDS OF PRESSURE HEAD h, VOLUME OF SECONDARY AND DRIVING WATER, AND THEIR PROPORTIONALITY FACTOR μ AS OBTAINED IN PRINCIPAL TESTS

h (m)	G (kg/s)	μ
5.25	7.19	0
5.28	7.68	1.07
5.19	14.82	2.06
4.89	28.30	3.94

(c) Pitot tube.- The calibration of the pitot tube was effected in the free water jet produced by the driving jet, with mixing pipe removed, the pitot tube being supported so as to swing in the axis of the jet - in the longitudinal plane - or at any desired angle of setting with respect to the jet axis. It is rotatable about its axis in every position.

The pitot tube should have the following characteristics with respect to the recording of the two test quantities:

1. The total head should be indicated without falsification if possible, even in yawed flow (i.e., when the flow direction is other than parallel to the pitot axis).

2. The static pressure indication should give a necessary correction in the simplest possible form, and be, as far as possible, independent of the yawed flow.

To meet the second requirement, it was necessary to study several forms before finding a suitable one.

The first attempt was to establish the limits within which the assumption, that the pressure of the surrounding air prevails in the jet, is justified. Figure 6 represents two test series giving the pressure on the jet axis. It is seen that the pressure balance is reached at a distance of about 1-nozzle diameter (30 mm) from the orifice. From this pressure it is assumed that it is equal to the pressure of the surrounding air.

All the calibrations enumerated hereinafter were planed so that the momentary test orifice of the pitot tube was placed at a point of the jet axis 50 millimeters distant from the mouth of the nozzle. The measured dynamic pressure corresponded very accurately to the speed computed for the total head from equation (2), where $\zeta = 0$ and $\epsilon^2 = 1/625 \sim 0$ for axis adjacent points. Yawed flow up to 12° and turning of the survey apparatus about its axis effect no change. Thus the first of the requirements is fulfilled.

Figure 7 shows the indicated static pressure head h_{st} plotted against the velocity head $h_d = c^2/2g$ for different angles β between jet and survey apparatus axis (different yawed flows). Two cases must be differentiated.

1. The flow may be diverted against the wide side ($\alpha = 90^\circ$), or

2. Against the small side of the apparatus ($\alpha = 0^\circ$).

The case $\alpha = 0^\circ$ is obviously unfavorable for a simple correction formula because of the substantial departure from proportionality existing between indicated static pressure head and velocity head even at $\beta = 3^\circ$. At $\alpha = 90^\circ$, on the other hand, h_{st} remains unchanged as function of h_d as far as $\beta \leq 6^\circ$, and even for $\beta = 9^\circ$ the calibration curve differs but little from that for $\beta \leq 6^\circ$ in the range of low velocities. As assumed for the present and also proved later on, this insensitivity to yawed flow extends over the greater part of the mixing field. In consequence, the calibration curve for $\beta \leq 6^\circ$ serves as a basis for the interpretation. Its equation is according to the measurements:

$$0.007\, h_d = h_{st} - h_{stw}$$

where h_{stw} is the true static pressure. The other relation reads

$$h_g = h_d + h_{stw}$$

where h_g denotes the total head recorded at the tip of the pitot tube. Then the desired quantities h_{stw}, h_d, and the velocity c follow at:

$$h_{stw} = \frac{h_{st} - 0.007\, h_g}{0.993} \tag{4}$$

$$h_d = h_g - h_{stw} \tag{5}$$

$$c = \sqrt{2\, g\, h_d} \tag{6}$$

In the course of the subsequent measurements it was found that the survey apparatus was apt to deviate from its calibration curve as a result of a slight variation in surface condition (material: brass). Hence, it was necessary to rub it slightly down with prepared chalk every few days and then rechalk the original curve by a second calibration measurement; the process was repeated, if necessary.

Mixing Field Survey

In conformity with the quantity ratios $\mu = 0$, 1, 2, and 4 of the secondary to the driving water volume, four series of tests were carried out, with about 1100 test points distributed in the mixing chamber for each series.

The survey started with the static pressure at successive points on the axis and on axially parallel straight lines, axially distant 20 millimeters corresponding to the identical distance from the tip of the pitot tube to the test orifices. Thus each position of the pitot tube yielded the indicated values for total head and static pressure for two different points in the mixing field. This fact was allowed for accordingly in the interpretation of the measurements.

These tests on axially parallel straight lines were usually placed at 10-millimeter radial distance partly above, partly below the pipe axis so as to spot any lack of symmetries. It was further found advisable to determine the pressure and velocity distribution more accurately by closely spaced test points in several cross sections, particularly

in the part of the mixing field adjacent to the driving nozzle, where velocity and pressure vary substantially with the distance from the pipe axis.

Prior to each measurement the two ducts in the pitot tube and the manometer tubing were blown out to expel air bubbles.

In spite of the damping devices installed in the test lines, the indicated pressures fluctuated very severely. Especially disagreeable were the irregular, protracted fluctuations which entailed observation periods of an average of 3 minutes.

Therefore the graphical representation of the explored mixing fields reproduced in the following should always be regarded with the limitation that the quantities represented in relation to the location are merely averages over comparatively long-time intervals.

Interpretation of Measurements and Test Data

The representation of the pressure field is predicated upon the assumption of some chosen reference pressure, as for instance, the pressure γh_1 in the annular slot at the driving nozzle entrance (fig. 2). With h'_g and h'_{st} denoting the read-off water column levels of the principal test corresponding to the pressure at the tip and at the orifices of the survey apparatus (all levels h being measured with respect to atmospheric pressure), there is obtained

$$h_{st} = h'_{st} - h_1; \qquad h_g = h'_g - h_1$$

Pressure and velocity are computed by equations (4), (5), and (6) and then plotted against the distance from the driving nozzle entrance for equal distances from the axis. Then a number of axially normal sections are traced through the mixing chamber and for these also the measured pressure and velocity distribution is plotted point by point, special attention being paid to the cross sections with the closely spaced test points.

In the following the pressure corresponding to the value h_{stw} is is indicated with p ($p = \gamma h_{stw}$). Figure 8 shows the pressure and velocity in two cross sections chosen at random.

The next problem is to complement the pressure and velocity distribution established point by point by a continuous area. This makes it necessary to fix a rule by which certain irregularities of the measured curves are smoothed.

At greater values for ratio μ it was found that the results of a number of the surveyed cross sections were not exactly symmetrical with the axis of the mixing pipe. The ratios were plotted at exaggerated scale, as in figure 9, where $\overline{AA}$ is the geometric axis of the mixing pipe, with the points 0_1, 0_2, 0_3, and so forth. The points 1, 2, 3, 1', 2', and 3' are intersection points of the surveyed velocity curves with parallels to the axis of abscissa. The points M_1, M_2, and M_3 divide the distances $\overline{11'}$, $\overline{22'}$, and $\overline{33'}$ in equal parts. For the further interpretation the line through M_1, M_2, and M_3, and so forth, was bent straight and regarded as axis. The asymmetry is, moreover, slight; the distance of this axis from the line $\overline{AA}$ is, at the most, 1.5 millimeters. The cause of this irregularity may lie in the asymmetry of the inflow for the secondary water; minor defects in the shape of the mixing pipe may contribute; a deflection of the pitot tube would also act in this direction.

The asymmetries existing in the pressure curves were smoothed in the same manner. In the area adjacent to the nozzle the measured pressure distributions over cross sections frequently showed a form as reproduced in figure 10. The measured minimum pressures are not alike by otherwise pressure curve symmetry. In such cases the arithmetic mean value serves as pressure peak for the interpretation. The cause of this irregularity may, aside from irregular inflow, be due to the scattering of the test points, which is comparatively great at these very points. The explanation for this unusual pressure minimum will be given elsewhere.

Figures 11 and 12 represent sections through the pressure and velocity areas for mixing ratio $\mu = 2$; figure 13, the pressure distribution in individual sections, and figure 14, the velocity profiles for $\mu = 2$ (x = distance from driving nozzle). Once the longitudinal and cross sections are definitely fixed, these two sets of curves define the pressure and velocity areas. For lucid representation these areas are intersected by a series of parallel planes, the analytical expression of which is $p = \text{constant}$, and $c = \text{constant}$. The section curves are represented in figures 15 to 18. The streamlines can be determined by graphical integration on the basis of the measured velocity profiles.

The streamlines are determined on the simplified assumption that the measured velocity, with sufficient accuracy, shall be equal to its axial component ($c \approx c_{ax}$). At the points of maximum inclination of the streamlines the difference between velocity c and axial component c_{ax} is 3 to 4 percent for $\mu = 0$, considerably less for $\mu = 1$, 2, 4. The secured streamlines are also shown in figures 15 to 18.

Error in the Static Pressure Record at Points of Great Velocity Gradient

Both Schlichting (reference 2) and Förthmann (reference 1) have already pointed out that the static pressure readings obtained in flows

with pronounced lateral velocity field are defective. The principal cause is most likely to be found in the strong pulsating transverse velocities accompanying such flows; as is evident from the calibration curves in figure 7, the survey apparatus is not insensitive to this yawed flow. The static pressure record is smaller than assumed in the utilized calibration curve. But it is somewhat unusual that, according to Förthmann (reference 1), these negative pressures can amount to as much as 15 percent of the impact pressure of the maximum speed in the test cross section,[1] as against only about 1 percent in the present case.[2] Approximately the same value was obtained with a survey apparatus of circular cross section 6 millimeters in diameter and lateral test orifices.

Figure 10 shows the form of the discussed negative pressure maximums. It most likely is a defective measurement and for the following reason: since the streamlines in this area are nearly parallel and straight, obviously, the pressure on normals can vary but little. The pressure measurement on the axis is correct or practically so, because the interchange of masses is very small. The probable pressure distribution is therefore somewhat as indicated by the dashed curve in figure 10. This probable pressure distribution in the separate sections is plotted so as to form a continuous surface (dashed curve in figs. 15 to 18).

Experiments with Driving Nozzle Extending Deeper into the Mixing Chamber

The position of the driving nozzle relative to the inlet of the mixing pipe may raise the suspicion that with the chosen arrangement the total rise is adversely affected insofar as the start of intermingling occurs in an area where certainly some irregularity of flow still exists. It therefore seemed desirable to measure the wall pressures with a nozzle extending farther into the mixing chamber in order to detect any eventual variation of the pressure field.

Figure 19 shows the lengthened and the normal nozzle. For the

---

[1]It is not quite clear from the cited reference whether this 15 percent refers to the local impact pressure or to that of the maximum speed in the test cross section. The second interpretation is rather the logical one.

[2]The greatest negative pressure peaks occur in cross sections in which the core of the driving jet has not as yet disintegrated; the maximum speed in these sections is therefore identical with the discharge velocity of the driving jet from the nozzle.

tests with the normal nozzle the pressure γh_1 in the annular slot of the nozzle (fig. 2a) served as reference pressure. Between this pressure and pressure γh_2 (test station, fig. 1) the following relation exists

$$\gamma(h_2 - h_1) = a$$

a assuming a specific value for each mixing ratio. Now, however, this pressure cannot be measured directly and is therefore calculated from the above relation; a is taken from the previous tests, h_2 is read off, as usual.

The tests indicate that the pressure rise with long driving nozzle is very similar to that obtained with short nozzle, except for being shifted backward for the excess length of 120 millimeters of the long nozzle. The somewhat unfavorable inflow for the start of the mixing with short nozzle has therefore no adverse consequences on the total pressure rise.

THEORY

Simplified Assumption and Method of Solution

An attempt was made, at first, to make mixing processes of the kind serving as basis of the experimental study, amenable to theoretical treatment by means of Prandtl's shearing stress formula, but these attempts were frustrated by mathematical difficulties. Then it was attempted to make flows which approached the explored mixing flows as closely as possible, amenable to theoretical study by simplifying assumptions.

In the following the intermingling of a jet with a parallel flow acting in the same direction by axially symmetrical arrangement and the assumption of constant pressure over the mixing field is treated as a flow of this kind. As for the previously computed mixing flows (references 3, 4, 2, 1), the following assumptions are made:

1. The mixing processes in cross sections with varying distances from the start of mixing shall be geometrically and mechanically similar.

2. The mixing path l shall be constant over a cross section and, therefore, proportional to the width of the mixing zone[1] for

[1] Assumptions 1 and 2 were originally made by Prandtl (reference 5).

different cross sections, according to the first assumption. The procedure is briefly as follows: assumptions 1 and 2 in conjunction with the impulse theorem themselves make it possible to find a law for the increase in width of the mixing field (as in references 4 and 2 but originally shown in reference 5). Herewith is suggested a formula for the velocity, which, together with Prandtl's shearing stress formula, reduces the employed simplified equation of motion to a common differential equation, the solution of which presents no difficulty.

Solution

(a) The Prandtl shearing stress formula.- In side-by-side flow of layers of density ρ with a velocity gradient largely perpendicular to the principal velocity, the interchange of momentum introduces an apparent turbulent shearing stress, which is expressed by

$$\tau = \rho l^2 \left(\frac{\partial u'}{\partial y}\right) \left|\frac{\partial u'}{\partial y}\right| \tag{7}$$

where u' is the average local velocity in x-direction, y the coordinate at right angles to it, and l the convection path. The average local transverse velocity v' of the mixing process, which causes the momentum interchange, is proportional to

$$l \frac{\partial u'}{\partial y}$$

hence

$$v' \sim l \frac{\partial u'}{\partial y} \tag{8}$$

(b) Formula for the velocity.- From the similarity of the state of flow in different cross sections follows

$$l = \alpha b \tag{9}$$

and for similarly placed points of different cross sections the proportionality relation

$$\frac{\partial u}{\partial y} \sim \frac{u}{b}$$

α is a proportionality factor, b the width of the mixing field, u the relative velocity in respect to the parallel flow of velocity U; hence

$$u' = U + u \text{ and whence } \frac{\partial u'}{\partial y} = \frac{\partial u}{\partial y}$$

With it and equations (8) and (9): $v' \sim \alpha u$. In addition

$$v' = \frac{db}{dt} = \frac{\partial b}{dx}\frac{\partial x}{dt} = u' \frac{\partial b}{\partial x} = (U + u)\frac{\partial b}{\partial x}$$

The only case considered hereinafter is that where u is negligibly small relative to U, which is at least admissible for sufficient distance from where the mixing starts. Then

$$v' = U \frac{\partial b}{\partial x} \sim \alpha u \quad \text{or} \quad U\frac{db}{u} \sim \alpha dx \tag{10}$$

A relation between u and b for integrating equation (10) is afforded by the impulse formula, applied to the control space according to figure 20:

$$\frac{J}{2\mu\rho} = 2U \int_0^{b/2} uy\,dy \tag{11}$$

wherein one term u^2 is neglected against $2Uu$; J is the impulse of

the driving jet, only the increased velocity relative to the parallel flow coming in consideration as velocity portion. The integral is proportional to a product ub^2, when u is the value for different cross sections taken at similarly placed points. With it $u \sim n/b^2$ (m^3/sec) n being a constant. The integration of equation (10) then gives

$$x \sim b^3 \frac{U}{n} \qquad \text{or} \qquad x \sim \left(\frac{b}{s}\right)^3$$

where $s = (n/U)^{1/3}$ for short. Similarly placed points of different cross sections therefore are situated on curves of the family

$$\eta = \frac{y}{b} = \frac{y}{sx^{1/3}} = \text{constant} \tag{12}$$

The velocity formula suggested in this and similar cases (references 3, 4, 2)

$$u = Us\varphi(x)f(\eta) \tag{13}$$

where φ is a function of x and f a function of η, gives, in conjunction with the condition that according to equation (11) the impulse in each cross section has the same value, hence must be independent of x:

$$\varphi(x)\, x^{2/3} = \text{constant}$$

Herewith equation (13) is transformed as follows (the constant being now included in $f(\eta)$):

$$u = \frac{Us}{x^{2/3}} f(\eta) \tag{14}$$

(c) Integration of equation of motion.- Figure 21 represents a ring element of the explored flow which is bounded by stream surfaces and planes normal to the x-axis. The impulse formula for this element under the assumption of constant pressure reads:

$$dR - dB = 0 \tag{15}$$

dR signifying the increase of the frictional or shearing force in radial direction, dB the increase of momentum in axial direction. Discounting the minor slope of the streamlines relative to the axis, both expressions are developed by the continuity equation and the relations

$$dB = \frac{\partial B}{\partial x} dx; \qquad dR = \frac{\partial R}{\partial y} dy$$

where $B = mc$ (m = specific mass of flow, c = its velocity), $R = \tau 2\pi y dx$. So, finally, the equation of motion in "natural" coordinates reads

$$c \frac{\partial c}{\partial x} = \frac{1}{\rho y} \frac{\partial (\tau y)}{\partial y} \tag{16}$$

In view of the nearly axially parallel flow, $c \approx u'$ can be reasonably approximated to $c \approx u' = U + u$. This affords, with the effected omission of u relative to U:

$$U \frac{\partial u}{\partial x} = \frac{1}{\rho y} \frac{\partial (\tau y)}{\partial y} \tag{17}$$

The expressions for u and τ, according to equations (7) and (14), are now written in this equation, whence, with the use of equation (12) and the relation

$$l \sim b \sim sx^{1/3} \qquad \text{or} \qquad l = ksx^{1/3} \tag{18}$$

where k denotes an as yet unknown quantity,

$$\frac{1}{3}\left[2f(\eta) + f'(\eta)\eta\right]\eta = k^2 \frac{\partial[\eta f'^2(\eta)]}{\partial\eta}$$

or (19)

$$(2\eta f + \eta^2 f')d\eta = 3\,k^2 d(\eta f'^2)$$

f' being the derivation of f with respect to η. The equation can be integrated once:

$$\eta^2 f - 3k^2\eta f'^2 = C \tag{20}$$

For $\eta = 0$ follows $C = 0$, since f and f' remain finite:

$$\eta f - 3k^2 f'^2 = 0 \tag{21}$$

Equation (21) can be integrated after separating the variables:

$$f = \left(\frac{\eta^{3/2}}{3\sqrt{3k}} + C_1\right)^2 \tag{22}$$

The constant C_1 follows from the boundary condition that for $u = 0$, η itself has a well defined value η_o. For $u = 0$, $f(\eta)$ is obviously also equal to 0, hence

$$C_1 = -\frac{\eta_o^{3/2}}{3\sqrt{3k}} \tag{23}$$

Equation (22) then reads:

$$f(\eta) = \left[\frac{1}{3\sqrt{3k}}(\eta^{3/2} - \eta_o{}^{3/2})\right]^2 \tag{24}$$

A further boundary condition defines the still unknown quantity s and the limiting value η_o: the difference of the impulses over each axially normal plane upstream and downstream from the driving jet entrance must yield the impulse J of the driving jet. Hence, according to equations (11), (14), and (24):

$$J = 4\pi\rho \int_0^{\eta_o} U^2 s^3 \left(\frac{1}{3}\frac{\eta^{3/2}}{\sqrt{3k}} + C_1\right)^2 \eta \, d\eta \tag{25}$$

The impulse J and the temporarily undetermined s are constants. Since η and k are dimensionless the formula can be written

$$J = \rho U^2 s^3$$

This necessarily specifies compliance with the condition

$$1 = \frac{4\pi}{(3\sqrt{3k})^2} \int_0^{\eta_o} (\eta^{3/2} - \eta_o{}^{3/2})^2 \, \eta \, d\eta$$

whence:

$$\eta_o = 1.756 \, k^{2/5} \tag{25a}$$

and, with the use of equation (23):

$$C_1 = -0.448 \, k^{-2/5}$$

Then the complete expression of the velocity u is:

$$u = \frac{U\left(\frac{J}{\rho U^2}\right)^{1/3}}{x^{2/3}} \left[\frac{1}{3\sqrt{3k}} \left(\frac{y}{\left(\frac{J}{\rho U^2} x\right)^{1/3}} \right)^{3/2} - 0.448\, k^{-2/5} \right]^2 \qquad (26)$$

The boundary of the affected zone has, according to equation (25a), the form

$$y_o = \left(x \frac{J}{\rho U^2} \right)^{1/3} 1.756\, k^{2/5} \qquad (27)$$

From equation (26) the velocity distribution in a section perpendicular to the axis then follows suitably dimensionless as quotient u/u_a, u_a being the velocity in the axis. Put for the sake of simplification,

$$\frac{U\left(\frac{J}{\rho U^2}\right)^{1/3}}{x^{2/3}} = H$$

the velocity on the axis is

$$u_a = HC_1^2$$

and put, furthermore, $\eta = \delta\eta_o$, where δ may assume any numerical value from 0 to 1, there is obtained

$$\frac{u}{u_a} = (\delta^{3/2} - 1)^2$$

The computed velocity profile is represented in figure 22.

COMPARISON OF CALCULATION AND EXPERIMENT

Decrease of Velocity on the Axis and Increase of Width of the Mixing Field

According to equation (26) the velocity on the curves η = constant decreases conformably to a power law. This decrease should be particularly easy to verify for the axis ($\eta = 0$). According to a similar, simple power law the width of the mixing zone increases with the distance from the point where the mixing starts, equation (27). Both laws are developed on the premise of constant pressure in the mixing chamber without considering boundary walls.

Because of the substantial pressure rise occurring in the measured mixing field, the velocity must naturally drop much faster than obtains by a calculation on the assumption of constant pressure, and the increase in mixing zone width in the cylindrical pipe also will differ from that in the unlimited parallel flow. Therefore it is not a priori possible to find these theoretical laws realized in the executed measurements. And in consequence it is also impossible to define from these tests the theoretically indeterminable constant k empirically in its order of magnitude.

For the case of mixing of a round jet with the surrounding still air the ratio l/y_o can be taken from the tests with the value 0.0738, according to Tollmien (reference 3). On the assumption that l/y_o shall be 0.0738, equations (12), (18), and (25a) give the value $k \approx 1/30$.

Form of Velocity Profiles

Although the assumptions for theory and test differ, the form of the measured velocity profiles suggests a comparison with the theoretically computed velocity distribution. Of course, this involves only cross sections of the mixing chamber in which

1. The sound, unmixed core of the driving jet is already completely gone and for which

2. The mixing motion has not advanced too close to the wall proximity, so that it is still logical to define a theoretical inflow velocity U of the delivered water:

$$U = \frac{G_2}{\gamma(F_r - F_o)}$$

G_2 (kg/sec) is the delivered quantity of water, F_r the mixing pipe cross section, and F_o the driving jet cross section at the exit from the driving nozzle. Figure 22 shows, aside from the computed velocity distribution, several of the measured velocity profiles for $\mu = 1$. It is seen that an acceptable agreement exists between theory and test throughout the particular zone, in spite of the fact that the theoretical assumption that μ should be small compared to U, does not hold for the cross sections employed for the comparison.

APPROXIMATE ANALYSIS OF THE MIXING PROCESSES

Flügel's Method

In Flügel's article (reference 6) on the calculation of jet apparatus, a dragging force effective between driving jet and entrained jet is presented in an unusually simple manner. Figure 23 shows a driving jet which entrains the surrounding fluid through mixing motions. For simplicity it is assumed that in each cross section the velocity c_2 of the delivered medium and the velocity c_1 of the driving jet shall be constant. The effective dragging force dR on a surface portion dO of the boundary area between driving and entrained jet shall then be:

$$dR = \chi \frac{\gamma}{2g} (c_1 - c_2)^2 \, dO$$

χ is a kind of friction coefficient. Next, the impulse formula is applied to a small sector of the driving jet and the delivered jet. After various transformations a differential equation is obtained which, among others, is solvable also for the assumption of constant throughflow cross section F and thus makes it possible to compute the velocity ratio c_2/c_1; that is, the degree of mixing for different distances from the start of mixing. The final formulas according to Flügel's report, are briefly introduced:

$$(K_1 - K_2)\sqrt{\frac{c_{10}}{2}}\,x = a_1\left(\sqrt{\frac{c_{10}}{c_{1x}}} - 1\right) - a_2\rho_0\left[\left(\frac{c_{10}}{c_{1x}}\right)^{3/2} - 1\right]$$

$$+ a_3\left[\frac{\sqrt{\frac{c_{10}}{c_{1x}}}}{1 - \rho_0\frac{c_{10}}{c_{1x}}} - \frac{1}{1 - \rho_0}\right] + \frac{a_4}{\sqrt{\rho_0}}\ln\frac{\left(1 + \sqrt{\rho_0\frac{c_{10}}{c_{1x}}}\right)\left(1 - \sqrt{\rho_0}\right)}{\left(1 - \sqrt{\rho_0\frac{c_{10}}{c_{1x}}}\right)\left(1 + \sqrt{\rho_0}\right)} \qquad (28)$$

$$c_{2x} = \frac{G_2 c_{1x}}{F\gamma c_{1x} - G_1} \qquad (29)$$

$$\Delta p = \frac{G_1}{gF}(c_{10} - c_{1x}) - \frac{G_2}{gF}(c_{2x} - c_{20}) - \lambda\sqrt{\frac{\pi}{F}}\frac{\gamma}{g}c_{20}\,c_{2x}\,x \qquad (30)$$

Herein:

c_{10} driving jet velocity
c_{20} velocity in entrained jet
} at reference cross section A-A (fig. 24)

c_{1x} driving jet velocity
c_{2x} velocity of entrained jet
} at distance x from the reference cross section

$$K_1 = \chi\sqrt{\pi\frac{\gamma}{G_1}}$$

$$K_2 = \sqrt{\pi\,\lambda\,k_2^2}\sqrt{\frac{\gamma}{G_1 + G_2}}\left(\frac{\rho_m}{1 - \rho_m}\right)\sqrt{\rho_m}$$

$$\rho_m \approx \sqrt{\rho_o \rho_x}$$

$$\rho_o = \frac{G_2 + G_1}{F \gamma c_{1o}}$$

$$\rho_x = \frac{G_1 + G_2}{F \gamma c_{1x}}$$

$$a_1 = k_1 (1 + k_2)$$

$$a_2 = \frac{k_1}{3}(k_1 - k_2)$$

$$a_3 = \frac{k_2^2}{2}$$

$$a_4 = \frac{k_2^2}{4}$$

$$k_1 = \frac{G_1}{G_1 + G_2}$$

$$k_2 = \frac{G_2}{G_1 + G_2}$$

$$k_3 = k_1 k^2_2$$

G_1 quantity of driving water

G_2 quantity of delivered water

Δp pressure rise relative to pressure in reference cross section

F cross section of pipe

λ coefficient of friction for the pipe wall (assumed for the numerical calculation at $\lambda = 0.005$)

Verification of the Dragging Force of the Driving Jet

The survey of the velocity field and the pressure field in the mixing chamber can serve as basis for an empirical prediction of the friction coefficient χ from equation (28). The calculation is especially simple for mixture ratio $\mu = 0$, the quantities a_3 and a_4 of equation (28) are equal to zero in this case. The velocity

$$c_{1x} = c_{2x} = G_1/\gamma F$$

in the smoothed cross section is then computed and from the representation of the pressure and velocity field the distance x from the start of mixing where velocity and pressure may be regarded as smoothed, is ascertained. Everything in equation (28) is then known except the looked for χ.

A similar attempt for the case of $\mu = 1$, 2, and 4, encounters the difficulty that the expression $\rho_0 c_{10}/c_{1x}$ in the smoothed cross section becomes equal to unity. Then the third and fourth term of equation (28) become infinitely great; that is, the equation states that uniform velocity occurs only for infinite pipe length.

To determine χ in these cases, select mixing field sections of not quite completed velocity compensation and read off an average velocity value for the area of the driving jet from the surveyed velocity profile, which then, entered as c_{1x}, together with the distance x of the particular cross section in equation (28), makes it possible to compute the value χ. The choice of cross sections should not go too far in the area of the almost smoothed zone, else the expression $\rho_0 c_{10}/c_{1x}$ approaches unity too much and the denominators of the third and fourth terms become almost zero; hence an inaccuracy of the read-off term acts comparatively very falsifying on the result.

Table 2 contains the computed χ in two reference sections, each for the four mixture ratios.

TABLE 2.- VALUES χ IN TWO REFERENCE SECTIONS EACH

μ	0	1		2		4	
x (m)	0.95	0.80	0.90	0.90	1.00	1.15	1.35
c_{1x} (m/sec)	.30	1.10	.80	1.40	1.15	1.70	1.50
χ	.102	.093	.119	.087	.108	.10	.127

So for the use of equation (28) a value of $\chi \approx 0.1$ should be reasonable.

The Pressure Rise

The pressure rise is preferably obtained by calculating the respective value x from equation (28) for a number of the assumed values c_{1o}/c_{1x}; the value $\chi = 0.1$ is utilized. After c_{2x} is computed by equation (29) the respective Δp is then found from equation (30).

Figure 25 shows the pressure distribution measured along the wall of the mixing pipe and that computed by the cited method. As regards the total pressure rise, good agreement obtains between theory and test, except for the fact that the measured pressure curves are considerably shifted into the mixing chamber as compared to the calculated curves. For the case $\mu = 0$ the theoretical pressure rise is slightly less than actually obtained by the measurement. This might be due to the fact that for this case an exceptionally heavy vortex ring is formed in the forward part of the mixing chamber, the forward and backward flowing part of which contributes impulses in the sense of an increased pressure rise (fig. 24). The same conditions are to be found to a lesser extent for $\mu = 1$.

The pressure rise computed for $\mu = 0$ presents another unusual feature; that is, the curve $\Delta p = f(x)$ (see equation (30)) exhibits a vertical tangent at point $x = 0.978$, or, in other words, the cited x-value represents a regular maximum of the curve $x = f(c_{1o}/c_{1x})$ (see equation (28)) at the point $c_{1x} = G/(\gamma F)$. This part of the pressure curve is reproduced at the right-hand side of figure 25. The dashed branch of the curve for $c_{1x} < G/\gamma F$ has no longer any physical meaning.

The pressure measured along the mixing pipe wall represented in figure 25 is not, as heretofore, referred to the pressure γh_1 at the driving nozzle entrance, but, like the calculated pressure rise, referred to the pressure p^* in the reference section A-A (fig. 24). A-A was placed at the start of the cylindrical mixing pipe to ensure the simplest possible application of c_{2o}. The driving nozzle may be visualized as being lengthened up to the section A-A, so that for the inlet impulse at velocity c_{1o}, the (numerically very small) increase due to the pressure drop $(\gamma h_1 - p^*)$ must be taken into consideration.

The determination of p^* proceeds from the recorded pressure γh_2; the equation of energy gives the pressure drop Δp_{2e} due to the velocity increase from test point to inlet cross section.

Hence:

$$\Delta p_{2e} = \gamma h_2 - p^* = \frac{\gamma}{2g}(c^{*2} - c_2^2)$$

With the assumption that the mixing pipe section through contraction as a result of the somewhat unfavorable form of inlet, as well as the existence of the ring vortex, is blocked by about 1/3, the following values for Δp_{2e} are obtained:

μ	0	1	2	4	
Δp_{2e}	0	8	32	116	mm of water column

Then, if the recorded pressure difference $\gamma(h_2 - h_1)$ for each mixing ratio is denoted by a, the difference between the previous and the presently employed reference pressure is

$$\gamma h_1 - p^* = \Delta p_{2e} - a$$

The subsequent compilation contains the test values a and the desired differences

μ	0	1	2	4	--	
a	0	4	10	26	mm	of water column
$(\Delta p_{2e} - a)$	0	4	22	90	mm	

Hence, to arrive at the pressure rise plotted in figure 25, the value $(\Delta p_{2e} - a)$ must be added to the pressures shown in figures 15, 16, 17, and 18.

Translation by J. Vanier,
National Advisory Committee
for Aeronautics.

REFERENCES

1. Förthmann, E.: Turbulent Jet Expansion. NACA TM No. 789, 1934.

2. Schlichting, H.: Über das ebene Windschattenproblem. Ing.-Archiv, Bd. 1, 1930, pp. 533-571.

3. Tollmien, Walter: Calculation of Turbulent Expansion Processes. NACA TM No. 1085.

4. Swain, L. M.: On the Turbulent Wake behind a Body of Revolution. Proc. Roy. Soc. London, ser. A, vol. 125, 1929, p. 647.

5. Prandtl, L.: Über die ausgebildete Turbulenz. Verhandl. 2. International Kongress für tech. Mech., Zürich 1926 (Zürich and Leipzig), 1927, pp. 62-74.

6. Flügel, Gustav: Calculation of Jet Apparatus. NACA TM No. 982, 1941.

BIBLIOGRAPHY

Trüpel, Th.: Über die Einwirkung eines Luftstrahles auf die umgebende Luft. Z. ges. Turbinenwes. Bd. 12, 1915, pp. 52-56, 66-70.

Zimm, Walter: Über die Strömungsvorgänge im freien Luftstrahl. VDI-Forschungsheft No. 234, 1921.

Prandtl, L.: Bericht über Untersuchungen zur ausgebildeten Turbulenz. Z.f.a.M.M., Bd. 5, 1925, pp. 136-139.

Wein, W., and Harms, F.: Handb. Exp. Physik. Bd. IV., pts. 1 and 4, (Leipzig), 1931.

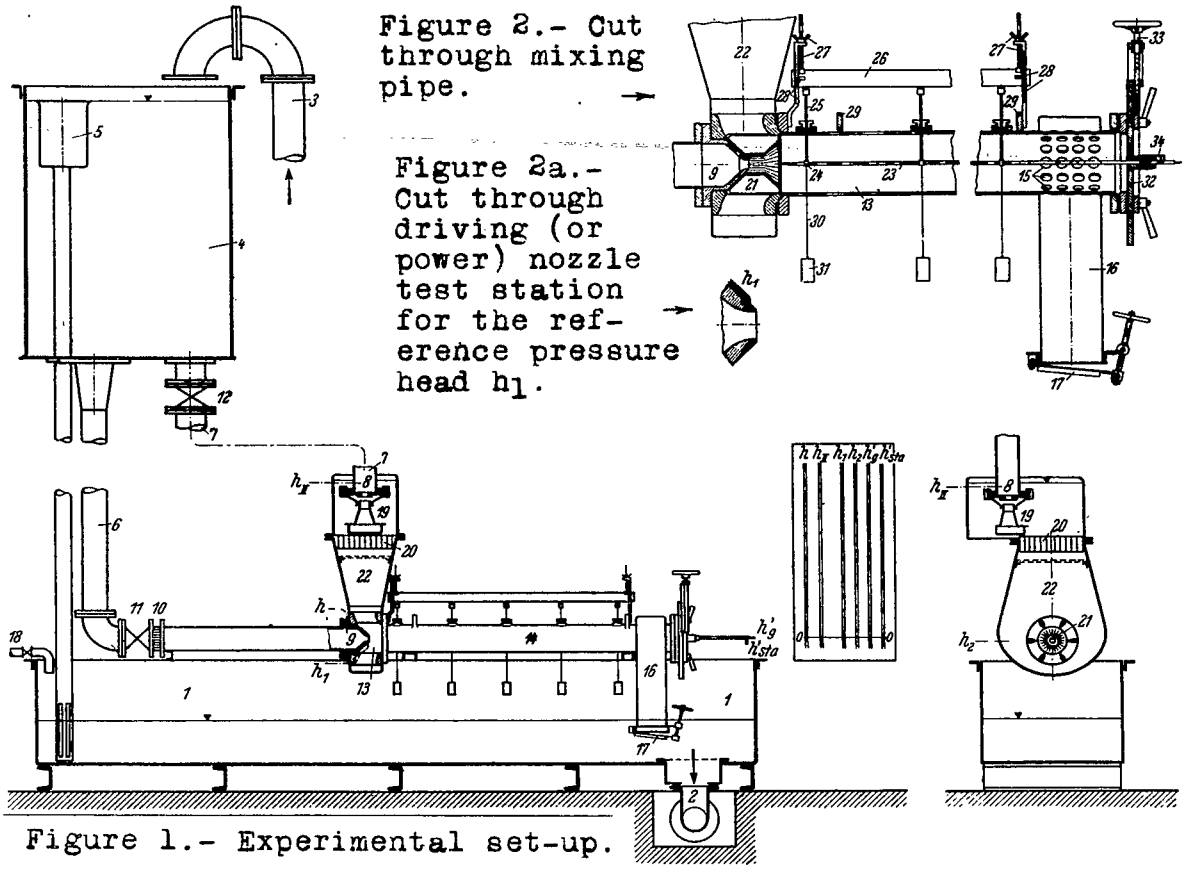

Figure 1.- Experimental set-up.

Figure 2.- Cut through mixing pipe.

Figure 2a.- Cut through driving (or power) nozzle test station for the reference pressure head h_1.

1, tank; 2, intake line to pump; 3, pressure line from pump; 4, overhead tank; 5, overflow; 6, downpipe to driving nozzle; 7, downpipe for secondary water; 8, test nozzle for secondary water; 9, driving nozzle; 10, straightener; 11, stop valve; 12, stop valve; 13, mixing chamber; 14, mixing pipe; 15, orifices in mixing pipe (fig. 2); 16, deflection branch; 17, throttle valve; 18, inlet from water piping; 19, small swash tank; 20, straightener and screens; 21, straightener with radial ribs (fig. 2); 22, inflow tank for secondary water; 23, pitot tube (fig. 2); 24, suspension rings; 25, brass strips; 26, iron beam; 27, nut and lead screw; 28, scale and pointer for reading level; 29, stops for control of level; 30, tension wire; 31, tension weight; 32, plate with stuffing box; 33, hand wheel for raising and lowering plate; 34, pointer for axial displacement of the pitot tube.

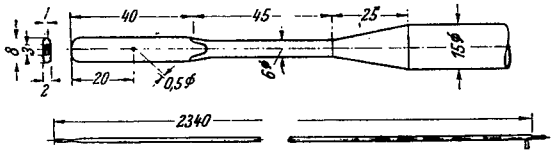

Figure 3.- Pitot tube and tip.

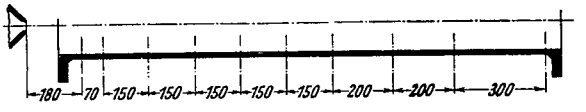

Figure 4.- Disposition of test orifices.

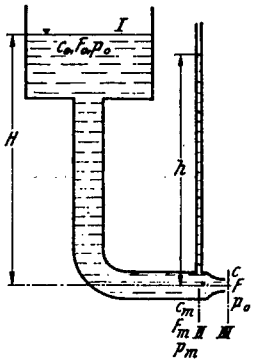

Figure 5.- Calibration set-up.

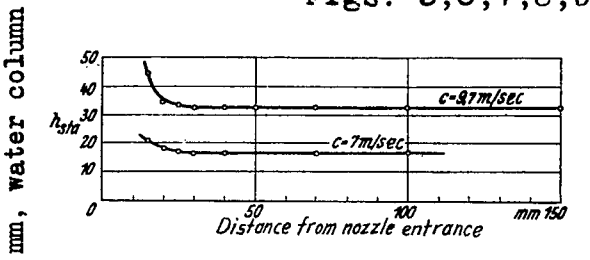

Figure 6.- Static pressure reading at various distances from the nozzle entrance.

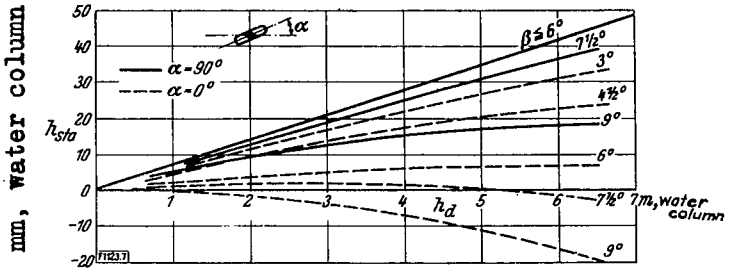

Figure 7.- Static pressure reading plotted against dynamic pressure at different yawed flows (β = angle of flow, α = angle torsion about axis of survey apparatus).

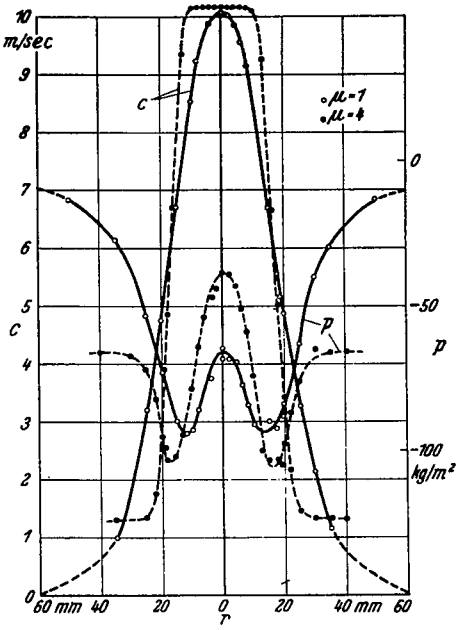

Figure 8.- Velocity and pressure profiles for $\mu = 1$ and $\mu = 4$.

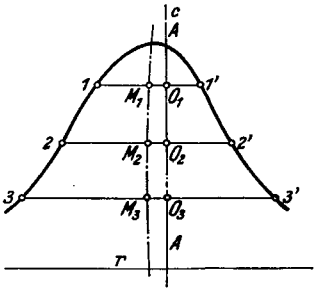

Figure 9.- Schematic representation of the asymmetry at measured velocity profiles.

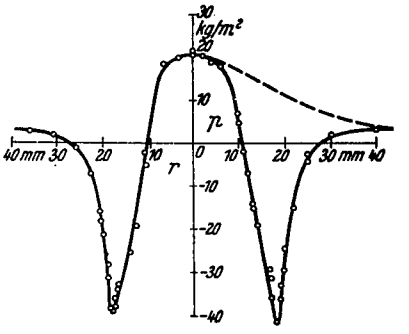

Figure 10.- Pressure profile near driving nozzle; the probably correct pressure is indicated by dashes.

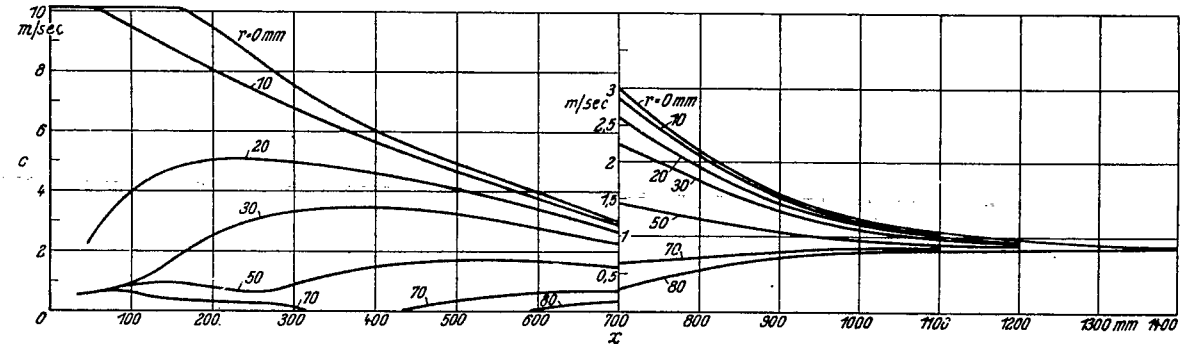

Figure 11.- Velocity distribution over the length of the mixing field at different distances from the axis (section through the velocity areas) for $\mu = 2$.

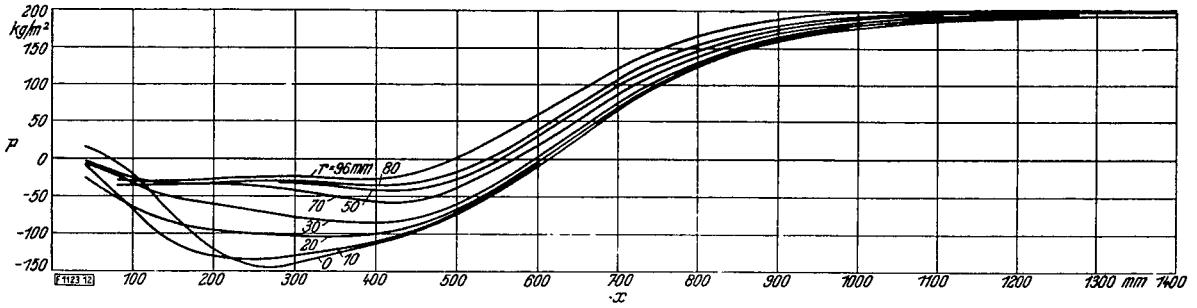

Figure 12.- Pressure rise over the length of the mixing field at different distances from the axis (section through the pressure areas) for $\mu = 2$.

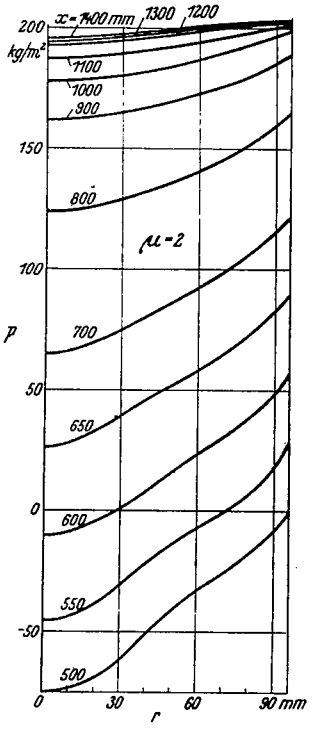

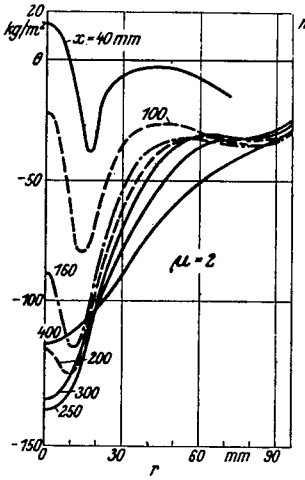

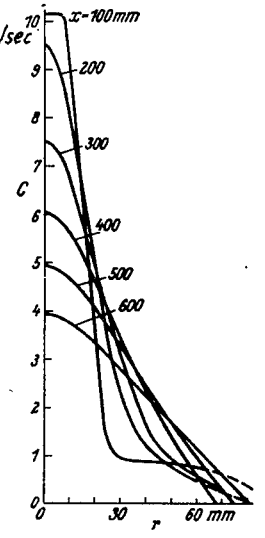

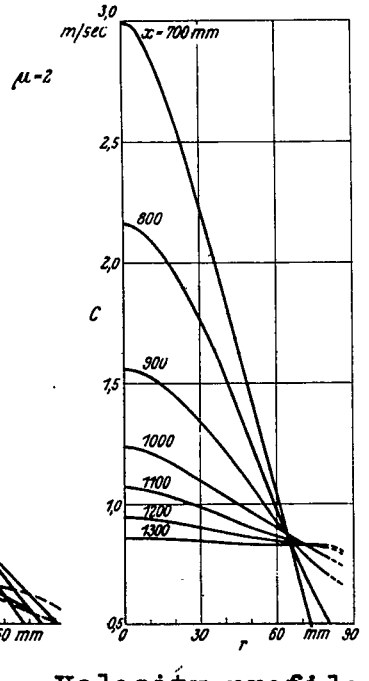

Figure 13.- Pressure distribution in individual sections of the mixing chamber for $\mu = 2$.

Figure 14.- Velocity profiles in the individual sections of the mixing chamber for $\mu = 2$.

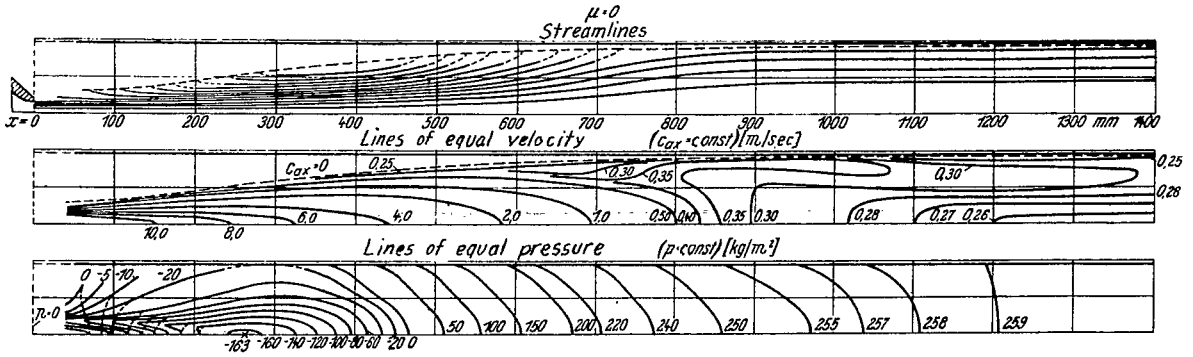

Figure 15.- μ = 0.

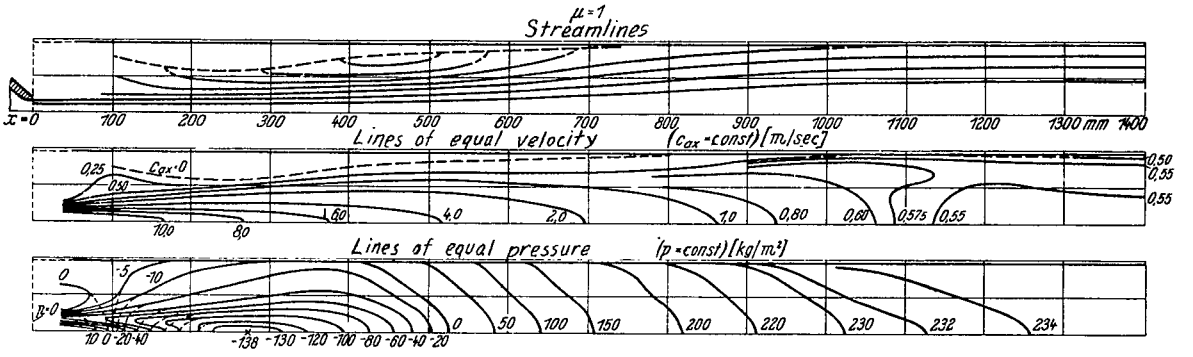

Figure 16.- μ = 1.

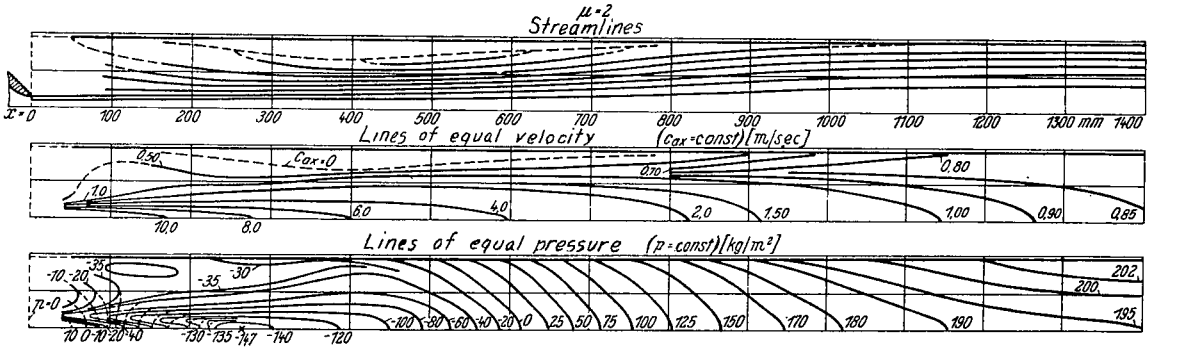

Figure 17.- μ = 2.

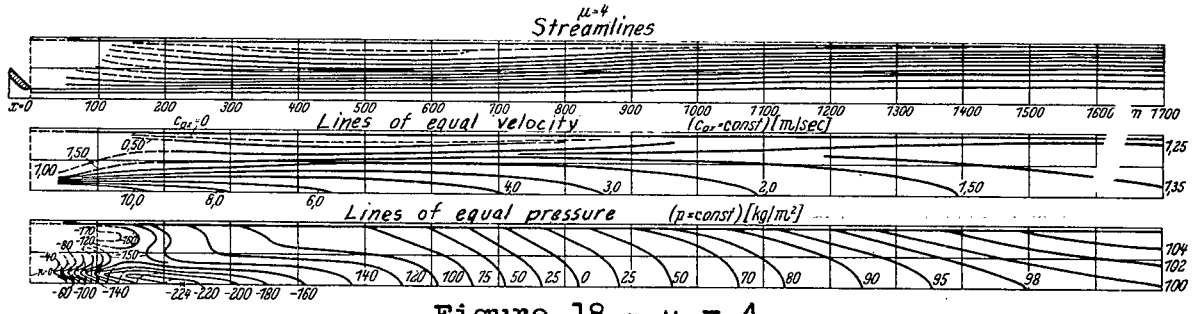

Figure 18.- μ = 4.

Figures 15 to 18.- Pressure and velocity distribution over the mixing field and variation of streamlines for different μ.

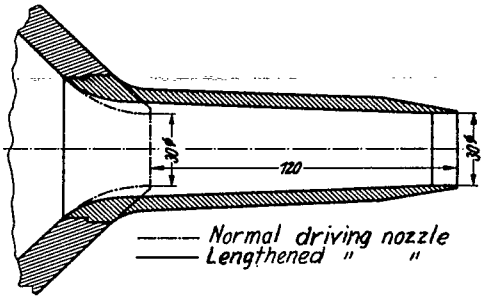

Figure 19.- Normal and lengthened driving nozzle.

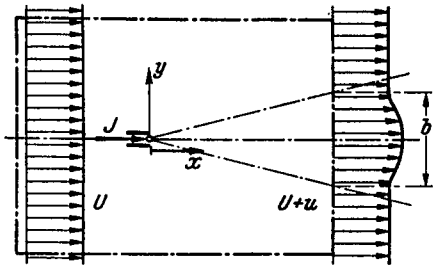

Figure 20.- Control space for applying equation (11).

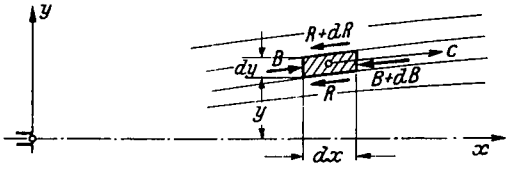

Figure 21.- Annular element with the applied forces.

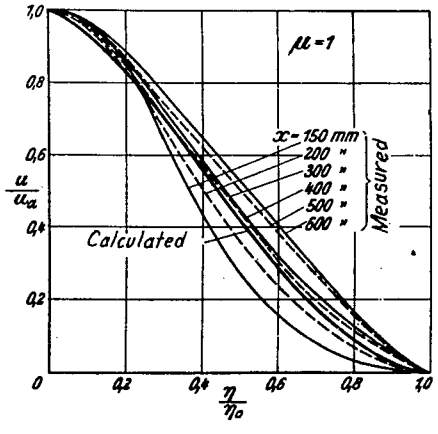

Figure 22.- Calculated and measured velocity profiles ($\mu = 1$).

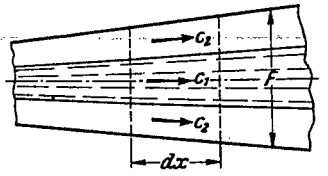

Figure 23.- Schematic sketch of driving jet, which entrains the surrounding medium as a result of mixing motion (from Flügel report).

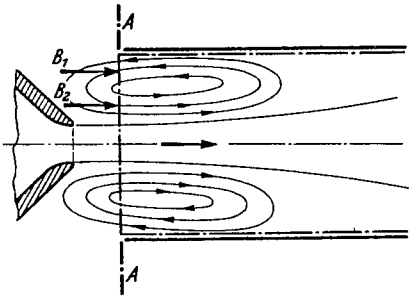

Figure 24.- Ring vortex with impulse contribution in the sense of increased pressure rise for in and outflowing portion.

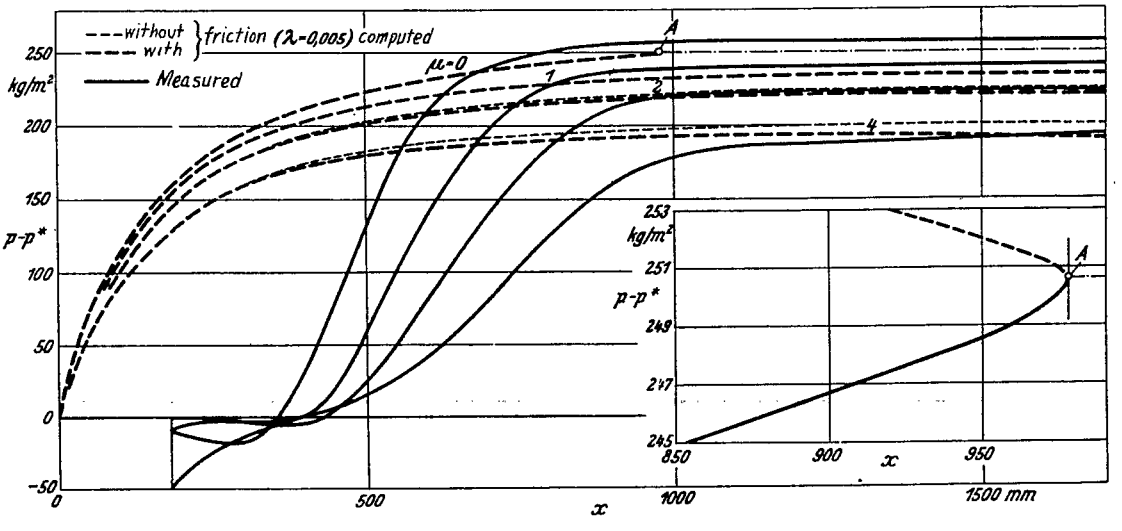

Figure 25.- Measured and calculated pressure rise.